RESEARCH ARTICLE

Key Points:
- High-resolution dissolved Fe and Al from Antarctica to the Bay of Bengal
- Mixed layer dissolved Al reflects meridional dust deposition gradients
- Atmospheric model and Al-based estimates of total deposition are compared

Supporting Information:
- Text S1
- Table S1
- Table S2

Correspondence to:
M. M. Grand,
maxime@hawaii.edu

Dust deposition in the eastern Indian Ocean: The ocean perspective from Antarctica to the Bay of Bengal

Maxime M. Grand[1], Christopher I. Measures[1], Mariko Hatta[1], William T. Hiscock[2], Clifton S. Buck[3], and William M. Landing[4]

[1]Department of Oceanography, University of Hawaii, Honolulu, Hawaii, USA, [2]Thermo Fisher Scientific, North Ryde, New South Wales, Australia, [3]Skidaway Institute of Oceanography, University of Georgia, Savannah, Georgia, USA, [4]Department of Earth, Ocean, and Atmospheric Science, Florida State University, Tallahassee, Florida, USA

Abstract Atmospheric deposition is an important but still poorly constrained source of trace micronutrients to the open ocean because of the dearth of in situ measurements of total deposition (i.e., wet + dry deposition) in remote regions. In this work, we discuss the upper ocean distribution of dissolved Fe and Al in the eastern Indian Ocean along a 95°E meridional transect spanning the Antarctic margin to the Bay of Bengal. We use the mixed layer concentration of dissolved Al in conjunction with empirical data in a simple steady state model to produce 75 estimates of total dust deposition that we compare with historical observations and atmospheric model estimates. Except in the northern Bay of Bengal where the Ganges-Brahmaputra river plume contributes to the inventory of dissolved Al, the surface distribution of dissolved Al along 95°E is remarkably consistent with the large-scale gradients in mineral dust deposition and multiple-source regions impacting the eastern Indian Ocean. The lowest total dust deposition fluxes are calculated for the Southern Ocean ($66 \pm 60 \, \text{mg m}^{-2} \text{yr}^{-1}$) and the highest for the northern end of the south Indian subtropical gyre (up to $940 \, \text{mg m}^{-2} \text{yr}^{-1}$ at 18°S) and in the southern Bay of Bengal ($2500 \pm 570 \, \text{mg m}^{-2} \text{yr}^{-1}$). Our total deposition fluxes, which have an uncertainty on the order of a factor of 3.5, are comparable with the composite atmospheric model data of Mahowald et al. (2005), except in the south Indian subtropical gyre where models may underestimate total deposition. Using available measurements of the solubility of Fe in aerosols, we confirm that dust deposition is a minor source of dissolved Fe to the Southern Ocean and show that aeolian deposition of dissolved Fe in the southern Bay of Bengal may be comparable to that observed underneath the Saharan dust plume in the Atlantic Ocean.

1. Introduction

The availability of Fe is central to the dynamics of carbon and macronutrient cycling in high-nutrient low-chlorophyll (HNLC) regions of the oceans and may regulate N_2 fixation in oligotrophic waters [*Boyd et al.*, 2007; *Falkowski et al.*, 1998; *Moore et al.*, 2009]. Considering that the deposition and partial dissolution of mineral aerosols constitute a major source of dissolved Fe to remote regions of the open ocean [*Jickells et al.*, 2005], establishing the pattern and magnitude of dust deposition in the remote ocean is required in order to evaluate its impact on nutrient and carbon cycling. Dedicated sampling for trace elements on selected sections of the U.S. Climate Variability and Predictability (CLIVAR)-CO_2 Repeat Hydrography Program has constituted an unprecedented opportunity to investigate the influence of atmospheric deposition on the biogeochemical cycles of bioactive trace elements in the remote upper ocean [*Grand et al.*, 2014]. The determination of dissolved Al and Fe on these CLIVAR sections can be used to resolve the geographic distribution and magnitude of dust deposition, its influence on the surface inventory of dissolved Fe, and to ascertain the accuracy of atmospheric model deposition estimates in the remote ocean.

The contribution of atmospheric deposition to the inventory of dissolved Fe in the upper ocean has been a matter of considerable debate in recent years, particularly in the HNLC Southern Ocean, where multiple-source terms are at play, measurements of total deposition (i.e., wet + dry) are rare, and atmospheric model estimates differ greatly in their estimates of total deposition [*Tagliabue et al.*, 2014a]. Using deposition data from the model of *Fan et al.* [2006], *Cassar et al.* [2007] argued that the input of aerosol Fe exerts a first-order control on productivity and export production in present-day subantarctic waters. The view was rapidly challenged on the

basis that the dust deposition model of *Fan et al.* [2006] had not been validated with field observations and was parameterized for Northern Hemisphere atmospheric conditions that may not be applicable to the remote Southern Ocean [*Boyd and Mackie*, 2008]. In addition, there is substantial observational evidence that margin sediments significantly contribute to the inventory of dissolved Fe available for biological uptake in Southern Ocean waters, particularly in the vicinity of the Antarctic Peninsula [*de Jong et al.*, 2012; *Measures et al.*, 2013; *Hatta et al.*, 2013] and in the wake of the Crozet and Kerguelen archipelagos in the Indian sector of the Southern Ocean [*Bucciarelli et al.*, 2001; *Blain et al.*, 2001, 2008; *Planquette et al.*, 2007, 2011; *Chever et al.*, 2010]. The importance of sediments in regulating the upper ocean inventory of Fe and carbon export in the Southern Ocean is also well supported by several biogeochemical models [*Moore and Braucher*, 2008; *Lancelot et al.*, 2009; *Tagliabue et al.*, 2009, 2014a; *Wadley et al.*, 2014], suggesting that the coupling between dust supply and export production observed by *Cassar et al.* [2007] in the Southern Ocean may be coincidental.

The scarcity of deposition observations in the Southern Ocean hinders the validation of atmospheric model estimates. Nevertheless, even where observations have been made, there is disagreement in the total deposition estimates. Near Kerguelen Island, total dust deposition has been estimated using the concentration of aerosols measured in the marine atmospheric boundary layer and assumptions with regards to dry deposition velocities and wet scavenging ratios to determine both the wet and dry components of total deposition [*Wagener et al.*, 2008]. More recently, by collecting both wet and dry depositions in two continuously open funnel collectors deployed over a 2 year period at Kerguelen Island, *Heimburger et al.* [2012] calculated a total deposition flux nearly 20 times higher than the shipboard aerosol estimates of *Wagener et al.* [2008]. *Heimburger et al.* [2012] suggested that since dust is transported above the marine atmospheric boundary layer near Kerguelen Island, *Wagener et al.'s* [2008] computation of wet deposition based on scavenging ratios of dust particle concentrations at sea level is probably an underestimation, thereby yielding underestimated total deposition fluxes. Clearly, many more observations are needed in remote oceanic regions to better quantify the magnitude of total deposition and reduce the uncertainty of atmospheric model deposition estimates, which are extensively used as input functions in global biogeochemical Fe models [e.g., *Tagliabue et al.*, 2014a]. Ideally, such a comparison should be performed with in situ data from a broad range of depositional environments and a variety of techniques to minimize methodological biases.

Given the dearth of island-based monitoring stations in the remote ocean and the logistical difficulty in maintaining them for extended periods, indirect estimates of total dust deposition constitute the best available way to determine the pattern of deposition in the remote ocean. Three methods have typically been used: the first is based on extrapolations of long-term, land-based deposition data [e.g., *Duce et al.*, 1991]; the second, described in the Kerguelen example above, relies on short-term shipboard aerosol collections near sea level [e.g., *Planquette et al.*, 2007; *Wagener et al.*, 2008; *Bowie et al.*, 2009]; and the third, which is the approach used in this paper, uses the concentration of lithogenic elements in surface waters to reconstruct the total amount of dust (i.e., dry + wet deposition) required to maintain these concentrations against scavenging removal [*Measures and Brown*, 1996; *Han et al.*, 2008; *Dammshäuser et al.*, 2011; *Hsieh et al.*, 2011]. While dissolved Ti and thorium isotopes have recently shown promise as a means to estimate dust fluxes to the surface ocean on time scales constrained by their residence times [*Dammshäuser et al.*, 2011; *Hsieh et al.*, 2011; *Hayes et al.*, 2013], *Measures and Vink* [2000] have shown that estimates of total dust deposition using surface-dissolved Al are in reasonable agreement with independent measurements of deposition in a variety of oceanic settings and depositional regimes.

This paper is concerned with the surface distribution of dissolved Al and Fe measured during two consecutive U.S. CLIVAR sections in the eastern Indian Ocean along a 95°E meridional transect spanning the Antarctic margin to the Bay of Bengal. We use the concentration of dissolved Al in the mean climatological mixed layer and a modified version of the Measurement of Al for Dust Calculation in Oceanic Waters (MADCOW) to estimate patterns of total dust deposition [*Measures and Brown*, 1996]. Using available estimates of the fractional solubility of aerosol Al and considering variations in the residence time of Al along the transect, we compute the total dust deposition fluxes and compare them with historical observations and composite model estimates of total deposition. We also calculate the aeolian flux of dissolved Fe using reported fractional solubility data of aerosol Fe to investigate the contribution of aeolian deposition to the inventory of dissolved Fe in the mixed layer of the Southern Ocean, south Indian subtropical gyre, and southern Bay of Bengal.
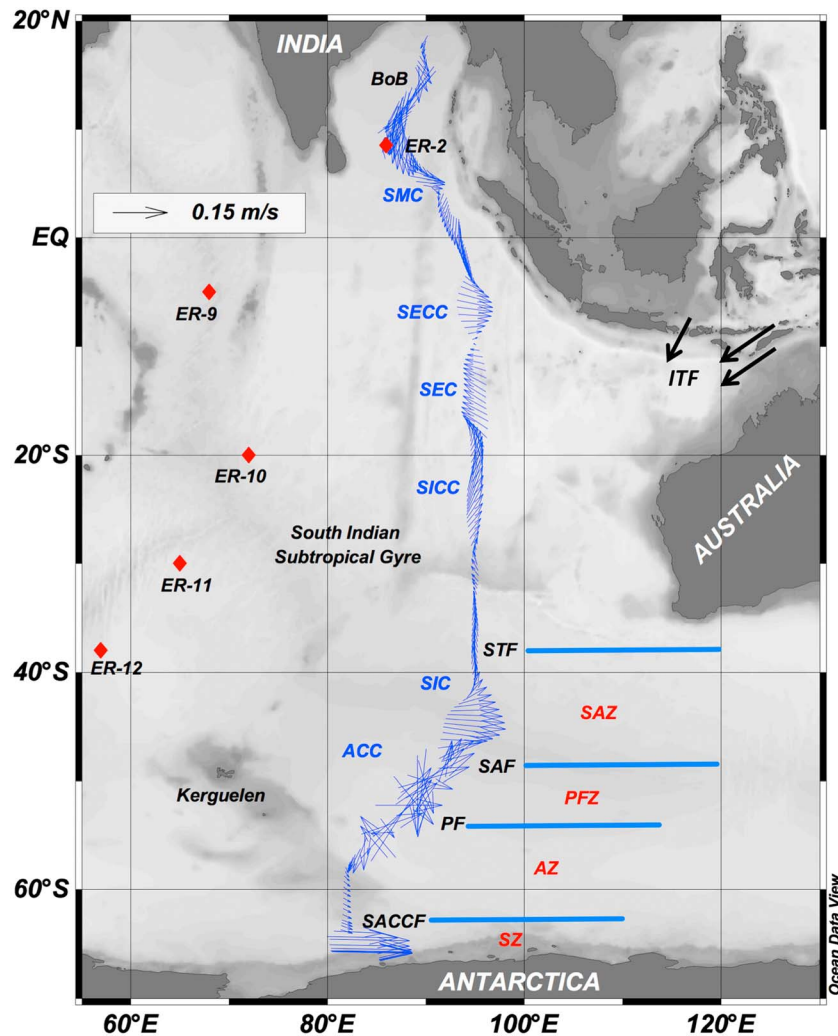
Figure 1. Near-surface circulation along the CLIVAR I08S and I09N cruise tracks. The thin blue arrows represent the upper mean 50 m LADCP velocities grouped into 1° bins. SZ: Southern Zone, SACCF: South ACC Front, AZ: Antarctic Zone, PF: Polar Front, PFZ: Polar Frontal Zone, SAF: Subantarctic Front, SAZ: Subantarctic Zone, STF: Subtropical Front, ACC: Antarctic Circumpolar Current, SIC: South Indian Current, SICC: South Indian Countercurrent, SEC: South Equatorial Current, ITF: Indonesian Throughflow, SECC: South Equatorial Counter Current, SMC: Southwest Monsoon Current, and BoB: Bay of Bengal. The red diamonds show the position of the stations sampled for dFe and dAl during the GEOTRACES-JAPAN expedition [*Vu and Sohrin*, 2013; *Nishioka et al.*, 2013].

2. Materials and Methods

2.1. Sample Collection and Analysis

Samples were collected aboard the R/V *Roger Revelle* during the U.S. CLIVAR CO_2 Repeat Hydrography I08S and I09N cruises. The I08S transect was occupied from 15 February to 13 March 2007, starting at the Antarctic continental shelf break and continuing northward until 28°S. Sampling along the I09N line began on 27 March 2007 at 28°S and was completed on 27 April in the Bay of Bengal (BoB) (Figure 1). A total of 85, 12-depth vertical profiles spaced at approximately 1° intervals were sampled along this cruise track, which extended from 65.8°S to 18°N, along 82–95°E. There are gaps in coverage near 55°S and 50°S in the Southern Ocean due to rough seas that prevented the deployment of the trace metal rosette from the stern of the ship. Since this paper is concerned with total dust deposition and its impact on upper ocean biogeochemistry, only data within the mean climatological mixed layer of each station are considered here (up to 185 m). The full-depth data set is described in detail in a companion manuscript [*Grand et al.*, 2015].

GRAND ET AL. 359

Seawater samples were collected using the trace metal clean system and sampling protocols described in *Measures et al.* [2008a]. Upon recovery, samples were filtered through acid-cleaned 0.4 μm polycarbonate track-etched membrane filters (Nuclepore #111107) and stored in the dark in 125 mL acid-cleaned polymethylpentene bottles until analysis was completed, usually within 48 h of collection. On the day of analysis, the samples were acidified to 6 mM with 6 M subboiled HCl, heated to 60 ± 10°C in a 900 W microwave oven to accelerate the release of complexed Fe, and allowed to cool to ambient temperature prior to analysis. Dissolved Fe and Al (hereinafter referred to as dFe and dAl) were determined using the flow injection analysis (FIA) methods of *Measures et al.* [1995] and *Resing and Measures* [1994], respectively. The FIA system was calibrated at regular intervals (3–4 h) using filtered, acidified (6 mM HCl), and microwaved surface seawater of low trace metal content spiked with commercial Fe and Al standards (Fisher Scientific). When necessary, the dFe and dAl data were drift corrected using the slopes of the calibration curves to compensate for the variations in instrumental sensitivity during the course of a day. The detection limits, defined as the 3σ variations of replicate 1 min loads ($n = 16$) of a Southern Ocean surface seawater sample, were 0.07 nM for dFe and 0.30 nM for dAl.

No detectable blank from the acid or sample buffer were found for Al. The dFe shipboard blank was quantified daily by spiking an acidified seawater sample with 80 μm ethylenediaminetetraacetic acid and analyzing it as the others. The resulting value was then subtracted from all dFe data produced on that day. The shipboard dFe blank was unusually high during the analysis of 13 consecutive stations between 41.5°S and 28.3°S, and applying this correction yielded slightly negative surface water values at some stations. Since replicate samples stored for shore-based inductively coupled plasma–mass spectrometry (ICP-MS) determination appeared to be contaminated for Fe [Pete Morton, personal communication, 2013], it was not possible to independently verify the magnitude of the dFe shipboard blank by correlating a subset of each day's shipboard run against ICP-MS data [*Measures et al.*, 2008b]. Thus, with no independent method to assess the accuracy of the shipboard blank correction, we are unsure of the validity of the data from 41.5°S and 28.3°S and excluded these data from the following discussion. Note that the SAFe intercalibration standards were not analyzed during either cruise, as the sample acidity is incompatible with our shipboard methodology. The dFe and dAl as well as the lowered acoustic Doppler current profiler (LADCP) and silicate (Si) data used in this contribution are publicly available on the CLIVAR and Carbon Hydrographic Office (CCHDO: http://cchdo.ucsd.edu) using the ExpoCodes 33RR20070204 and 33RR20070322 for the I08S and I09N stations, respectively.

2.2. Other Data Sources

Observed mixed layer depths (MLD$_{OBS}$) were computed using the density criterion of *de Boyer Montégut* [2004] using in situ conductivity-temperature-depth data for each cruise. The mean climatological mixed layer depths (MLD$_{CLIM}$) within a 1°×1° longitude and latitude bins of all stations were extracted from the Argo climatology of *Holte et al.* [2010]. On six occasions in the Southern Ocean, the MLD$_{CLIM}$ were extracted within a 2°×2° bin due to lack of Argo coverage. The annual total dust deposition estimates from a composite of three modeling studies were extracted within 1°×1° longitude and latitude bins from the I08S and I09N stations [*Mahowald et al.*, 2005, and references therein].

3. Results

In this section, the surface circulation of the study area is presented in relation to the distribution of surface dFe and dAl. To organize the discussion, the cruise track is divided into three hydrographic regimes (Figure 1): the Southern Ocean (65.8°S–38°S), which extends from the Antarctic margin to the subtropical front; the south Indian subtropical gyre and South Equatorial Countercurrent region (38°S–5°S); and the equatorial-BoB regime (5°S–18°N), which includes 18 stations in the BoB (5°N–18°N). Figure 2 shows the distribution of surface (~25 m) dFe and dAl, and Figure 3 shows the surface salinity and MLD$_{OBS}$ at each station along the transect. The distribution of dAl shows a meridional gradient in concentrations with uniformly low values in the Southern Ocean (0.3–1.33 nM) and higher levels at the northernmost stations of the BoB (up to 32 nM). Surface dFe, in contrast, showed a U-shaped distribution characterized by variable and elevated levels at the southern (up to 0.82 nM) and northern ends (up to 0.62 nM) of the transect and uniformly low values in the south Indian subtropical gyre ($<$0.2 nM; Figure 2).
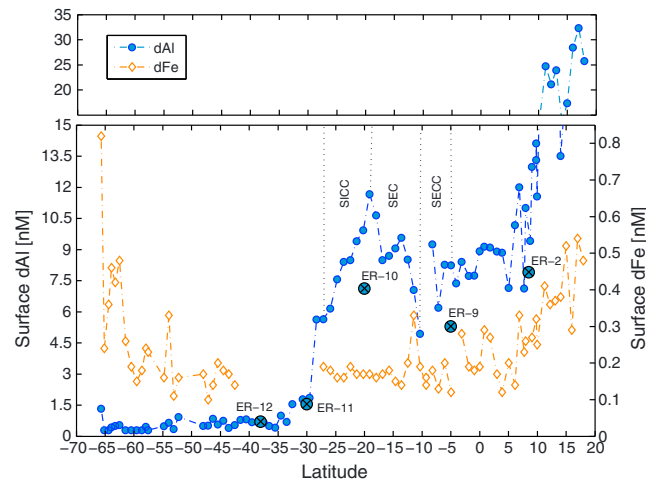
Figure 2. Surface dAl and dFe (<25 m) measured along the cruise track. Note the change in the dAl scale (top). The broken lines delineate the latitudinal bands of the major zonal currents in the gyre and SECC region. SICC: South Indian Counter Current (northeastward flow), SEC: South Equatorial Current (westward flow), and SECC: South Equatorial Counter Current (eastward flow). The circled crosses show the mean surface dAl values (<25 m) from *Vu and Sohrin* [2013]: ER-2: 8.5°N, 86°E; ER-9: 5°S 68°E; ER-10: 20°S 72°E; ER-11: 30°S 64°E; and ER-12: 38°S 57°E.

3.1. Southern Ocean (65.8°S–38°S)

The circulation of the Southern Ocean domain is dominated by the eastward flowing Antarctic Circumpolar Current (ACC). The ACC transport is concentrated along three fronts that separate zones with relatively uniform water mass properties. Using the property criteria of *Orsi et al.* [1995], we identified the South ACC Front (SACCF) at 63°S, the Polar Front (PF) from 57 to 54°S, and the Subantarctic Front (SAF) at 49°S. The ACC circulation is bounded to the north by the Subtropical Front (STF), near 40–38°S, and to the south by the Southern Boundary, which appears to merge with the SACCF along this section. The ACC fronts separate four zones [*Talley et al.*, 2011]: the Southern Zone (SZ) lying poleward of the SACCF, the Antarctic Zone (AZ) located between the SACCF and the PF, the Polar Frontal Zone (PFZ) between the PF and the SAF, and the

Subantarctic Zone (SAZ), which extends from the SAF to the STF (Figure 1). The SAZ near the cruise track experiences the deepest winter mixed layers of the South Indian Ocean, with depths generally exceeding 500 m in winter [*Rintoul and Bullister*, 1999; *Wong*, 2005].

Surface dAl levels in the eastern Indian sector of the Southern Ocean were extremely low (0.54 ± 0.25 nM, $n = 25$), and seven samples in this region had dAl levels less than or equal to the analytical detection limit (0.3 nM). The concentration of dAl increased northward (Figure 2), with significantly lower values south of the PF (66–54°S) relative to waters farther north (54–38°S) in the SAZ (two tailed t test, $p < 0.05$). These surface dAl values, which reflect minimal dust inputs in the circumpolar domain, are among the lowest reported in the world ocean and are consistent with surface observations in other sectors of the Southern Ocean that typically lie below 1 nM [*van Beusekom et al.*, 1997; *Measures and Vink*, 2000; *Obata et al.*, 2004; *Middag et al.*, 2011, 2012, 2013].
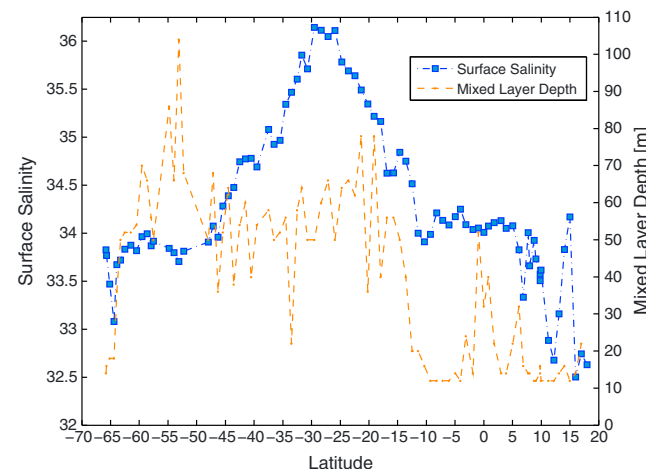
Figure 3. Surface salinity and observed mixed layer depth (MLD$_{OBS}$) along the cruise track.

Surface dFe exhibited an opposite meridional trend with values decreasing northward from 0.46 ± 0.22 nM ($n = 5$) in surface waters of the SZ to 0.16 ± 0.03 nM ($n = 7$) in the SAZ (Figure 2). We note that a similar meridional trend in dFe was also observed in a recent compilation of historical dFe data from the upper 100 m of the Indian sector of the Southern Ocean [*Tagliabue et al.*, 2012]. The elevated surface dFe values from the Antarctic margin to the PF (54°S) may reflect localized inputs from melting sea ice and icebergs [*Croot et al.*, 2004a; *Lannuzel et al.*, 2007, 2010; *Lin et al.*, 2011], as illustrated by the drop in surface salinity near 65°S (Figure 3). These elevated dFe levels could also reflect a lateral supply from shelf sediments

transported by strong alongshore currents (Figure 1) and/or upwelling of dFe-enriched waters from below [*de Baar et al.*, 1995; *Hoppema et al.*, 2003; *Sokolov and Rintoul*, 2007], followed by winter entrainment into the mixed layer [*Tagliabue et al.*, 2014b]. The mean dFe in all surface water samples of the Southern Ocean along the cruise track was 0.26 ± 0.16 nM ($n = 23$), within the range of surface dFe values reported in the Australian sector (0.14–0.63 nM [*Lannuzel et al.*, 2011; *Bowie et al.*, 2009]), the Atlantic sector along 6°E (0.19–1.46 nM [*Croot et al.*, 2004a]) and 0°E (0.1–0.3 nM [*Klunder et al.*, 2011]), in the mixed layer along 20°E (0.05–0.39 nM [*de Jong et al.*, 2012], and in the Pacific sector of the Southern Ocean (<0.15–0.3 nM [*Measures and Vink*, 2001]).

3.2. Subtropical Gyre and SECC Region (38°S−5°S)

The subtropical gyre of the South Indian Ocean extends from the eastward flowing South Indian Current (SIC) near 40°S to the westward flowing South Equatorial Current (SEC) near 15°S (Figure 1). The surface expression of the SEC, which carries fresh waters from the Indonesian Throughflow (ITF) region across the upper 300 m of the eastern Indian Ocean [*Gordon et al.*, 1997], was identified on this section as the band of westward velocities (Figure 1) and decreasing surface salinities from ~18 to 10°S (Figure 3). In the central part of the gyre (28–18°S), the northeastward flowing South Indian Countercurrent (SICC) dominates the surface circulation (Figure 1). The SICC, which flows against the prevailing winds, originates south of Madagascar and flows across the south Indian subtropical gyre near 25°S [*Reid*, 2003; *Siedler et al.*, 2006; *Palastanga et al.*, 2007].

Unlike the nearly featureless meridional dAl distribution of the Southern Ocean, the south Indian subtropical gyre is characterized by important fluctuations in surface dAl (Figure 2), which broadly coincide with east-west reversals in the surface circulation inferred from LADCP data along the cruise track (Figure 1). For example, the abrupt rise in surface dAl (1.9 to 11.7 nM) from ~29°S to 19°S coincides with the northeastward flow of the SICC (Figure 1). From 19°S to 10°S, the twofold decline in dAl corresponds with the position of the westward flowing SEC (Figure 1). North of 10°S, outside the limits of the south Indian subtropical gyre, the rise in dAl is associated with the eastward flowing South Equatorial Counter Current (SECC; Figure 1). Thus, nearly all variations in dAl concentrations in the gyre and SECC region coincide with zonal reversals in the LADCP velocities.

The only other dAl data reported from the south Indian subtropical gyre were collected during the GEOTRACES-JAPAN program [*Vu and Sohrin*, 2013; *Nishioka et al.*, 2013] (Figure 1). The mean surface dAl values (<25 m) at five stations sampled in December 2009 to the west of the present cruise track (57–72°E) are shown in Figure 2. Despite the ~2800 km separating the cruise tracks, both data sets show comparable meridional trends (Figure 2). However, in the central gyre and SECC region (ER-10 and ER-9), the surface dAl levels from the GEOTRACES-JAPAN expedition were significantly lower than the present study, possibly because the CLIVAR cruise track was closer to the dust source emanating from western Australia. In contrast to dAl, dFe levels in the gyre were remarkably uniform (Figure 2). The mean dFe in the gyre was 0.18 ± 0.03 nM ($n = 16$). Our values are significantly higher than the mean shipboard dFe reported by *Nishioka et al.* [2013] in the upper 25 m at stations ER-12, ER-11, and ER-10 of the GEOTRACES-JAPAN expedition (0.04 ± 0.008, $n = 6$). However, our mean dFe compares well with the mean dFe measured using shore-based ICP-MS on their stored replicate samples (0.14 ± 0.05 nM, $n = 6$ [*Vu and Sohrin*, 2013]).

3.3. Equatorial Regime and Bay of Bengal (5°S−18°N)

The oceanography of the tropical Indian Ocean and BoB is characterized by current systems and freshwater fluxes subjected to a strong monsoonal seasonality. We sampled the region during the spring intermonsoon (8–27 April 2007), when freshwater inputs from the Ganges-Brahmaputra and precipitation are at minima [*Prasanna Kumar et al.*, 2007; *Benshila et al.*, 2014]. At this time, we observed an ~40 m thick lens of low-salinity (<34) surface waters north of ~5°N (Figure 3). The low salinity and warm sea surface temperatures generate a strong stratification with shallow mixed layers, which impedes vertical transfer of nutrients by wind driven mixing in the BoB [*Prasanna Kumar et al.*, 2002]. Except for a narrow jet of eastward velocities near 5°N that could be interpreted as the Southwest Monsoon Current (SMC), southward flow predominated throughout the equatorial regime and BoB domains at the time of sampling (Figure 1). The most striking feature in the equatorial regime and BoB is the pronounced increase in surface dAl (7.1 to 26 nM) and dFe (0.2 to 0.5 nM) from 5°N until the northernmost station at 18°N in the BoB (Figure 2). This trend coincides with a significant drop in surface salinity (34.08 to 32.0; Figure 3). *Vu and Sohrin* [2013] reported mean surface dAl and dFe (<25 m) of 7.9 and 0.39 nM at station ER-2 in the southern BoB (Figure 1), which are comparable with our surface observations (9.42 nM for dAl and 0.30 nM for dFe) at one station of the cruise track located within 55.56 km of ER-2.

Eddy pumping is a potential means of disrupting the surface stratification of the BoB [*Prasanna Kumar et al.*, 2004; *Muraleedharan et al.*, 2007; *Sardessai et al.*, 2007]. On this section, the anomalous spike in salinity near 13–15°N (Figure 3), which is accompanied by a drop in surface dAl and an increase in surface dFe (Figure 2), is consistent with the presence of a cold-core eddy bringing saline, dAl-depleted and dFe-enriched deep waters to the surface waters of the BoB. Observation of sea surface height satellite imagery confirmed the presence of an elongated area of sea level depression near 17°N, 87°E (data not shown). Note that the spike in surface dAl centered at 6°N may be the result of the SMC carrying Arabian Sea surface water enriched in dAl across the cruise track (Figure 2).

4. Discussion

In the following, we will first describe the assumptions and limitations of applying the MADCOW model over the cruise track before using it to calculate the pattern of dust deposition in the three hydrographic provinces described above. The MADCOW total dust deposition estimates will then be discussed in relation to dust source regions, historical observations, and atmospheric model simulations and finally used to elucidate the biogeochemical implications of aeolian inputs of dFe to surface waters of the eastern Indian Ocean.

4.1. MADCOW Dust Deposition: Assumptions and Limitations

The essence of MADCOW is that the concentration of dAl in the mixed layer reflects the balance between the addition of dAl from the partial dissolution of mineral aerosols and its removal via particulate scavenging [*Measures and Brown*, 1996]. MADCOW therefore assumes steady state and only an atmospheric source of dAl. It also makes assumptions regarding the composition and solubility of aerosol Al, the mean residence time of dAl, and the depth of the mixed layer. In the following, we justify the rationale behind our choice of mixed layer depths (MLD), fractional solubility of aerosol Al, and residence time of dAl in the mixed layer.

In the original MADCOW model, *Measures and Brown* [1996] used a fixed 30 m MLD, because their dAl data were restricted to the tropical and subtropical Atlantic in the spring/summer time period. Applying a fixed 30 m MLD to our section is clearly not applicable considering the range of MLD_{OBS} along the cruise track (12–104 m; Figure 3). We therefore used the mean climatological MLD (MLD_{CLIM}) closest to each station along the cruise track, which we retrieved from a density-based MLD climatology that was assembled using Argo profiles from 2000 to 2011 [*Holte et al.*, 2010]. The mean Argo MLD_{CLIM} integrates seasonal variations that may bias our total deposition estimations if we had used the MLD_{OBS}.

The fractional solubility of aerosol trace elements appears to be determined by atmospheric chemical processing and is impacted by the abundance of acidic species, which are enhanced by fossil fuel combustion sources [*Baker and Croot*, 2010; *Kumar et al.*, 2010; *Measures et al.*, 2010; *Sholkovitz et al.*, 2012]. Thus, the use of a fixed fractional solubility constitutes an important source of uncertainty when applying MADCOW over an ocean section spanning regions remote from anthropogenic influences (i.e., the Southern Ocean) to areas close to heavily populated and industrialized regions (i.e., the BoB). Since there are no data available in the Indian Ocean from which we can develop regionally variable aerosol Al solubilities to use in MADCOW, we have assembled a database of measurements from the Pacific and Atlantic Oceans to determine the most suitable solubility for this section (Table S1 in the supporting information). Table 1 shows that operationally defined solubility estimates of aerosol Al span a wide range (0.1–49.6%) with the highest solubilities measured in the North Atlantic and the lowest solubilities in the Pacific Ocean. Since the transect considered in this study encompasses air masses with Atlantic-like (i.e., natural and anthropogenic dust influences) and Pacific-like (i.e., remote) characteristics, we took the geometric mean of all data of Table S1 in the supporting information (3.6%) and applied it to our section in an attempt to impose an Al solubility near the middle of the uncertainty range. We note that this value lies within the range of values used in the original MADCOW (1.5–5% [*Measures and Brown*, 1996]) but is lower than that produced by *Jickells* [1999] for the Sargasso Sea (4.4%) and the median Al solubility of *Baker et al.* [2006] for the Atlantic Ocean (9%).

The second largest uncertainty in the MADCOW deposition fluxes stems from the possibility of geographical variations of the residence time of dAl in the mixed layer. Dissolved Al is mainly removed from the upper ocean via passive scavenging onto sinking particles, which means that its residence time is inversely correlated with the concentration and flux of suspended particulate matter settling through the mixed layer [*Moran and Moore*, 1992]. In the upper ocean, the residence time of dAl, with respect to total dust deposition, has been estimated using the mean concentration of dAl and dust inputs retrieved from land-based, long-term

Table 1. Summary Statistics of the Fractional Solubility of Aerosol Al in the Pacific and Atlantic Oceans Including the Composite Solubility Used in This Study[a]

	Pacific Ocean	Atlantic Ocean	Composite (This Study)
Geometric Mean	2.7	12.6	3.6
Min	0.1	3.7	0.1
Max	15.9	49.6	49.6
n	126	30	158

[a]Statistics produced using the data of *Buck et al.* [2013, 2010], *Sato* [2002], and *Wuttig et al.* [2013]. See Table S1 in the supporting information for full data set. All solubilities are in percent.

deposition measurements as well as atmospheric model estimates. Using this approach, the residence time of dAl in the upper ocean has been estimated to range from ~0.5 to more than 15 years, with the shorter residence times observed in productive regions subjected to high deposition [*Schüßler et al.*, 2005; *Dammshäuser et al.*, 2011] and longer residence time in regions characterized with lower productivity [*Jickells* 1999; *Dammshäuser et al.*, 2011]. We have applied a uniform 5 year residence time to MADCOW to compute the total dust deposition fluxes from the Antarctic margin to the southern limb of the BoB at 5°N [*Measures and Vink*, 2000]. This value lies in the middle of the range of dAl residence times (1–8 years) estimated for this region using the Biogeochemical Elemental Cycling (BEC) ocean model, which simulates the oceanic distribution of dAl using dust fluxes from the Dust Entrainment and Deposition model [*Han et al.*, 2008]. The BEC model suggests that the residence time of dAl along our cruise track ranges from ~4 to 8 years south of 50°S and ~1 to 4 years north of 50°S in the Southern Ocean, 1 to 8 years in the south Indian subtropical gyre and SECC region and 1 to 2 years in the equatorial domain and BoB [*Han et al.*, 2008].

Considering that the BoB is characterized by high productivity and particulate sinking fluxes inferred from sediment trap studies [*Ramaswamy et al.*, 1997; *Stoll et al.*, 2007], the residence time of dAl in the BoB is probably significantly less than that in the oligotrophic subtropical gyre and Southern Ocean sectors of the cruise track, where we assumed a 5 year dAl residence time. In the BoB, *Srinivas and Sarin* [2013] recently published a dry deposition Al flux based on a shipboard aerosol sampling campaign covering the entire BoB during the period of continental outflow (January–April). Although their sampling period spanned only 3 months of the year, their data should still represent the near total annual aeolian Al flux to the BoB, since during the rest of the year, the winds blow predominantly onshore and do not support enrichment of air masses with continental aerosols [*Srinivas and Sarin*, 2013]. The inventory of dAl that we measured in the mixed layer of the BoB ($26 \pm 4\,m$) was $430 \pm 200\ \mu mol\ Al\ m^{-2}$. We calculate a soluble Al flux to the BoB of $390 \pm 240\ \mu mol\ Al\ m^{-2}\ yr^{-1}$ using *Srinivas and Sarin's* [2013] Al dry deposition flux of $0.8 \pm 0.5\ mg\ m^{-2}\ d^{-1}$ and a fractional solubility of 3.6%. Assuming steady state, this translates into a dAl residence time with respect to dust deposition of 1.1 ± 0.8 year in the mixed layer of the BoB, which compares well with the BEC model outputs of 1–2 years [*Han et al.*, 2008]. This value also lies within the range of dAl residence times (0.4–2.5 years) estimated for the northern Arabian Sea (>10°N) with respect to dust deposition and particle export [*Schüßler et al.*, 2005].

The modified MADCOW calculates total dust deposition using the following equation:

$$G = \frac{[Al] \times MLD_{CLIM}}{MRT \times S} \times 0.33 \tag{1}$$

where G is the total dust deposition flux in $mg\ m^{-2}\ yr^{-1}$, MRT is the mean residence time of dAl in the mixed layer (1.1 years in the BoB (>5°N) and 5 years elsewhere), S is the fractional solubility of aerosol Al (3.6%), and 0.33 is a factor that accounts for the mass ratio of Al in dust (8.1%), the molar mass of Al, and unit conversions. MLD_{CLIM} refers to the Argo mean climatological mixed layer depth closest to each station along the cruise track [*Holte et al.*, 2010], and [Al] is the mean dAl concentration (nM) in the MLD_{CLIM}. When more than one sample was collected within the MLD_{CLIM}, the dAl values were averaged. The numerical effects of equation (1) are such that halving the residence time or fractional solubility of aerosol Al at any given location will double the calculated dust input, while halving the depth of the mixed layer will reduce the calculated dust input by a factor of 2.

4.2. Uncertainties and Limitations in the Northern Bay of Bengal (>10°N)

It is difficult to quantify the uncertainty of our total deposition estimates since the variability of the fractional solubility of aerosol Al and residence time of dAl in the MLD_{CLIM} along our cruise track are not precisely known, except in the BoB (see section 4.1). Using the solubility data from Table S1 in the supporting information, we
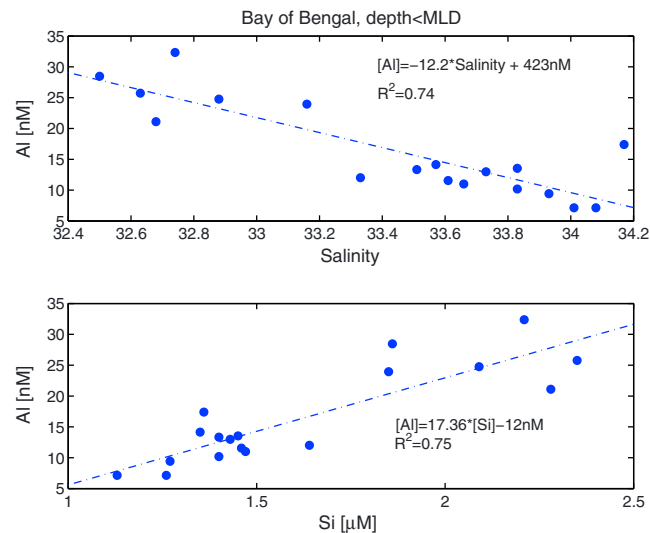
Figure 4. Relationship between dAl and salinity ((top) dAl = −12.2 ± 1.8 × Salinity + 423 ± 60.3) and dAl and Si ((bottom) dAl = 17.4 ± 2.5 × Si − 11.8 ± 4.2) in the MLD_{OBS} of the Bay of Bengal.

calculate that the fractional uncertainty of the Al solubility is about 200% (3.6 ± 6.8%, n = 158, ±2σ). Assuming that the fractional uncertainties of the MLD_{CLIM} and of the mean residence time of dAl in the MLD_{CLIM} are 20 and 300%, respectively, and neglecting the uncertainty of our dAl measurements (~2.5%), we can propagate errors in equation (1) and estimate that the uncertainty of our total deposition estimates is on the order of a factor of 3.5. In comparison, the uncertainty of the total dust deposition estimates based on the concentration of aerosols in the marine atmospheric boundary layer is on the order of threefold [*Duce et al.*, 1991], while the uncertainty of the atmospheric model estimates is likely to be a factor of 10 [*Mahowald et al.*, 2005].

In the northern reaches of the BoB (>10°N), eddy pumping and the large inflow of freshwater from the Ganges-Brahmaputra river system violate the assumptions in MADCOW that dust deposition and scavenging are the sole processes affecting dAl levels in the mixed layer. As shown in section 3.3, a cold-core eddy brought deep waters depleted in dAl to the surface at ~14–15°N. Our estimates of total dust deposition in this latitudinal band should thus be treated with caution. More significantly, we find that mixed layer dAl and salinity were negatively correlated and that dAl and Si were positively correlated in the BoB (Figure 4), suggesting that riverine inputs play a significant role in adding to dAl and Si there. Further support for the riverine source comes from the slope of the Al:Si relationship in the mixed layer of the BoB (~17 ± 2.5 nmol:μmol), which is close to the Al:Si (~10 nmol:μmol) ratio of river water, calculated using the mean world river concentration of Al of 1.5 μM of *Meybeck* [1988] and the mean river Si content of 150 μM of *Tréguer et al.* [1995]. Taken together, these considerations point to a significant riverine influence on MLD dAl, particularly in the northern reaches of the BoB (>10°N), where the highest surface dAl levels were observed (Figure 2) and the influence of the Ganges-Brahmaputra river plume should be most prevalent [*Vinayachandran and Kurian*, 2007; *Benshila et al.*, 2014]. Quantifying the relative importance of atmospheric and riverine sources to the inventory of dAl in the MLD of the northern BoB requires a first-order knowledge of the concentration of dAl in the river water end-member, the amount of dAl removed via scavenging during estuarine mixing, and the magnitude of mixing that the resulting freshwater plume is subjected to. Since such estimates are unavailable, it is not possible to correct the mixed layer dAl inventory of the northern BoB for the contribution of the Ganges-Brahmaputra river plume and use this to calculate a dust flux. Therefore, the northern BoB (>10°N) MADCOW estimates will not be considered in the following discussion.

Figure 5 shows the MADCOW-derived total dust deposition estimates overlaid with composite total deposition data from three aerosol models along the transect [*Jickells et al.*, 2005; *Mahowald et al.*, 2005]. Excluding the values from the northern BoB (>10°N), where the riverine contribution to MLD_{CLIM} dAl cannot be neglected or corrected for, our estimates of total dust deposition ranged from ~10 to 3500 mg m^{-2} yr^{-1} along the cruise track and show a pronounced meridional gradient, with the lowest values reported poleward of the PF and the highest near the northern limb of the subtropical gyre and in the southern BoB. Overall, both MADCOW and the composite model data produce comparable meridional patterns of dust deposition across the eastern Indian Ocean up to about 5°S, where model simulations predict a sharp northward increase in deposition that occurs farther north in our estimates (Figure 5).

4.3. Dust Deposition in the Southern Ocean (65.8°S−38°S)

The MADCOW total dust deposition fluxes in the Southern Ocean sector (10–290 mg m^{-2} yr^{-1}) were the lowest of the transect and showed a northward increase, with significantly higher inputs occurring north
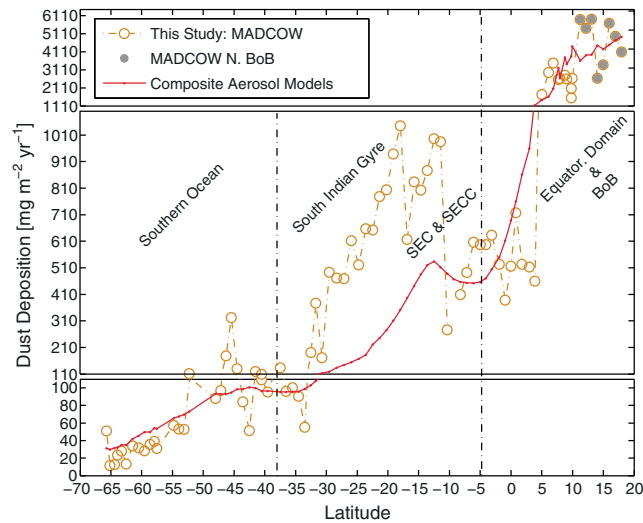
Figure 5. MADCOW total dust deposition overlaid with composite atmospheric model total deposition data along the cruise track. Model data are the mean of three reanalysis-based atmospheric models [*Jickells et al.*, 2005; *Mahowald et al.*, 2005]. The grey shading highlights the MADCOW estimations in the northern Bay of Bengal that are not at steady state due to riverine inputs from the Ganges-Brahmaputra river system and are excluded from the discussion (see text for details).

of the PF at 54°S (Mann-Whitney U test, $p < 0.01$; Figure 5). Higher deposition in the northernmost reaches of the Southern Ocean (>54°S: 100 ± 60 mg m^{-2} yr^{-1}) probably reflects long-distance transport of dust originating from South Africa [*Gaudichet et al.*, 1989; *Tanaka and Chiba*, 2006; *Mahowald*, 2007], combined with a possible local Kerguelen Island source. This trend is also seen in global dust models and extrapolations of land-based measurements [*Duce et al.*, 1991; *Mahowald et al.*, 2005]. Although Patagonian dust may also contribute to the northward increase in deposition observed in the Southern Ocean [*Tanaka and Chiba*, 2006; *Mahowald*, 2007; *Dammshäuser et al.*, 2011], recent observations along the meridional CLIVAR A16S section at ~30°W, where the bulk of Patagonian dust is shown to be deposited in atmospheric models, do not show any evidence of enhanced

surface dAl signals south of 20°S that could be attributed to the deposition of Patagonian dust [*Mariko Hatta*, personal communication].

Our mean Southern Ocean total dust deposition flux is ~3.6 times lower than that measured over a 2 year sampling period using open collectors collecting both dry and wet depositions at Kerguelen Island (Table 2). It is possible that the MADCOW estimations for the Southern Ocean underestimate the true flux, because the 3.6% solubility applied in MADCOW may be high for the Southern Ocean. In this regard, we note that three samples from the South Pacific (67.5–38°S) suggest that the fractional solubility of Al in this area was on the order of 1% [*Buck et al.*, 2013]. It is also possible that our total deposition flux is underestimated because of dilution of the mixed layer dAl signal during winter deep mixing leading to a residence time of dAl shorter than 5 years along our cruise track in the Southern Ocean [*Measures and Vink*, 2000; *Middag et al.*, 2013]. However, it cannot be ruled out that orographic rainfall at Kerguelen yields enhanced precipitation rates relative to our open-ocean study area. Considering that wet deposition appears to dominate total deposition (wet + dry) at Kerguelen [*Heimburger et al.*, 2012], the Kerguelen Island data may not be strictly comparable to

Table 2. Mean MADCOW Total Dust Deposition Fluxes and Comparisons to Atmospheric Model, Land- and Island-Based Extrapolated Measurements and Shipboard Aerosol Collection Estimates[a]

	Southern Ocean (66°S–38°S)	Gyre/SECC (38°S–5°S)	Equator (5°S–5°N)	Bay of Bengal (5°N–10°N)
This study: MADCOW	66 ± 60	480 ± 280	490 ± 80	2500 ± 570[f]
Atmospheric models[b]	67 ± 27	280 ± 170	700 ± 230	3000 ± 1000[f]
Land extrapolations[c]	10–100	10–1000	100–10,000	>10,000
Land-based measurements[d]	240			
Shipboard aerosol collection	14 ± 5[e]			300–6000[g]

[a]Data are mean $\pm 1\sigma$ or reported ranges in mg m^{-2} yr^{-1}. The 1σ represents the geographical variations in the flux and does not include uncertainties, which are on the order of a factor of 3.5.
[b]*Mahowald et al.* [2005].
[c]*Duce et al.* [1991].
[d]*Heimburger et al.* [2012].
[e]*Wagener et al.* [2008].
[f]Fluxes exclude data north of 10°N (see text for details).
[g]*Srinivas and Sarin* [2013].

Table 3. Estimated Fluxes of Dissolved Fe to the Surface Ocean Resulting From Total Aeolian Deposition (See Text for Details)[a]

Region	Aeolian dFe Flux (μmol (dFe) $m^{-2} yr^{-1}$)
Southern Ocean (66–38°S)	1.2 ± 1.1
Subtropical Gyre and SECC (38–5°S)	14 ± 8.0
Southern Bay of Bengal (5–10°N)	290 ± 70

[a]Data are mean $\pm 1\sigma$ in μmol (dFe) $m^{-2} yr^{-1}$. The reported 1σ reflects the geographical variations.

our open-ocean study area, which is ~1500 km downstream and should not be impacted by orographic rainfall caused by Kerguelen Island (1852 m maximum elevation).

Based on the limited shipboard aerosol observations, several investigators have claimed that atmospheric models overestimate total dust deposition in the remote Southern Ocean [*Wagener et al.*, 2008; *Bowie et al.*, 2009]. In contrast, we find that the mean MADCOW estimates and the composite model fluxes of *Mahowald et al.* [2005] along the cruise track were not significantly different (Mann-Whitney *U* test; Table 2), even though the model estimates are slightly higher than MADCOW south of 50°S (Figure 5). Similar to *Heimburger et al.* [2012], our data suggest that the total deposition flux of *Wagener et al.* [2008], based on aerosol shipboard sampling near Kerguelen Island, is too low (Table 2), probably as a result of the sporadic nature of dust fluxes and the limited duration possible for shipboard sampling. In addition, the computation of total deposition using aerosol concentrations in the marine atmospheric boundary layer may underestimate the total flux because wet scavenging at higher altitude may not be properly accounted for [*Heimburger et al.*, 2012]. In contrast, the multiyear residence time of dAl in the Southern Ocean means that our estimates integrate any seasonal variations in the magnitude of deposition. Our estimates also include the dry and wet components of dust deposition without underlying assumptions regarding deposition velocities or scavenging ratios.

Converting our mineral deposition fluxes into an estimate of aeolian dFe flux to the Southern Ocean requires knowledge of the fractional solubility of aerosol Fe. However, the scarcity of measurements of aerosol Fe composition and solubility in the Southern Ocean and the lack of consensus on a standardized leaching protocol to obtain aerosol Fe solubility values that most faithfully reproduce the dissolution of aerosol Fe in surface seawater [*Mahowald et al.*, 2005; *Baker and Croot*, 2010; *Sholkovitz et al.*, 2012] subject estimates of soluble aeolian Fe deposition to a considerable degree of uncertainty. We have assembled a database of solubility measurements south of 40°S using recent data from the Indian Ocean in the vicinity of the present cruise track [*Gao et al.*, 2013], data from the South Pacific Ocean collected during CLIVAR P16S [*Buck et al.*, 2013], as well as the compilation of *Sholkovitz et al.* [2012]. However, we excluded all data from the South Atlantic north of the latitude of Cape Horn (~56°S) to eliminate solubility measurements performed immediately downwind of continental influence since the eastern Indian sector of the Southern Ocean is remote from continents. We also excluded one data point from the Australian sector of the Southern Ocean suspected to be impacted by combustion aerosols [*Bowie et al.*, 2009]. The resulting data set consists of 40 measurements with solubilities ranging from 0.2 to 29.1% (Table S2 in the supporting information). We took the geometric mean of these measurements (2.9%) as our best estimate of the fractional solubility of Fe for the remote Southern Ocean (Table S2 in the supporting information). Using this value, the MADCOW total deposition estimates and assuming that the dust deposited contains 3.5% Fe (wt/wt), we calculate a mean dFe aeolian flux of 1.2 ± 1.1 $\mu mol\, m^{-2}\, yr^{-1}$ (range of 0.2 to 5.4 $\mu mol\, m^{-2}\, yr^{-1}$) to surface waters of the Southern Ocean (Table 3). These values are comparable to the dissolvable Fe flux range of 0.1–9.5 $\mu mol\, m^{-2}\, yr^{-1}$ estimated by *Gao et al.* [2013] in the vicinity of the present cruise track as well as the 0.9–2.7 $\mu mol\, m^{-2}\, yr^{-1}$ aeolian dFe deposition flux of *Bowie et al.* [2009] obtained farther east in the Australian sector of the Southern Ocean south of Tasmania. Our dFe flux is also comparable to recent BEC model simulations using different parameterizations of aerosol Fe solubility that yield 0.05–2.9 $\mu mol\, m^{-2}\, yr^{-1}$ [*Han et al.*, 2012] and recent MADCOW-based estimates (1.6 ± 0.7 $\mu mol\, m^{-2}\, yr^{-1}$) for the Pacific sector of the Southern Ocean along 150°W [*Measures et al.*, 2012]. However, our highest Southern Ocean dFe deposition flux estimate (5.4 $\mu mol\, m^{-2}\, yr^{-1}$) is nearly 10 times lower than the highest model simulations of *Fan et al.* [2006] (5–50 $\mu mol\, m^{-2}\, yr^{-1}$), possibly because the parameterization of aerosol solubility employed in that model, which is based on atmospheric sulfur chemistry, is not applicable to the Southern Ocean remote from the influence of anthropogenic emissions [*Boyd and Mackie*, 2008]. Our highest aeolian dFe flux for the Southern Ocean is also more than 30 times lower than the 180 $\mu mol\, m^{-2}\, yr^{-1}$ soluble Fe flux that *Heimburger et al.* [2013a] recently calculated for Kerguelen Island. The Kerguelen dFe flux was calculated using the total Fe deposition flux obtained using duplicate open

collectors [*Heimburger et al.*, 2013b] and applying a very high median solubility of 82% that was derived from the measurements of the soluble fraction of Fe from five rain events collected within the same period [*Heimburger et al.*, 2013a]. Although the works of *Heimburger et al.* [2012, 2013a, 2013b] do not appear to be experimentally compromised and do not include samples possibly compromised by local soils in their calculations, it is difficult to reconcile such a large dissolved Fe flux (almost 50% of that seen under the Saharan plume in the Atlantic [*Sarthou et al.*, 2003]) with the HNLC status and the generally low dFe concentrations that characterize surface waters of the Southern Ocean away from the shelf sediments and melting sea ice inputs [*Measures et al.*, 2012; *Tagliabue et al.*, 2012].

The deposition of our calculated aeolian dFe flux ($1.2 \pm 1.1\ \mu\text{mol m}^{-2}\text{yr}^{-1}$) into the Southern Ocean MLD_{CLIM} at the longitude of our observations (~60 m) would increase MLD_{CLIM} dFe by ~20 pM each year, which is ~7% of the mean dFe measured in the MLD_{CLIM} (0.27 ± 0.16 nM, $n = 23$) of all Southern Ocean stations occupied on the transect. Our mean Southern Ocean aeolian dFe flux is also nearly 20 times lower than the Southern Ocean deep winter mixing entrainment flux ($21.1\ \mu\text{mol m}^{-2}\text{yr}^{-1}$) of *Tagliabue et al.* [2014b]. These considerations strongly suggest that dust deposition is not the dominant annual source of dFe to surface waters of the eastern Indian sector of the Southern Ocean, although we cannot rule out that it might be important over short periods immediately after deposition. We conclude that upwelling/deep mixing inputs are likely the principal contributors to the inventory of dFe in the mixed layer of the eastern Indian sector of the Southern Ocean, as has been previously reported for the Pacific sector [*Measures and Vink*, 2001], with sedimentary and meltwater inputs also playing a role in some regions.

4.4. Dust Deposition in the South Indian Gyre and SECC Region (38°S−5°S)

In the gyre, the pattern of total dust deposition inferred from mixed layer dAl is remarkably consistent with dust model outputs, which predict a northward increase in the deposition across the gyre reaching a maximum near 12.5°S (Figure 5). However, the mean total deposition flux inferred from MLD_{CLIM} dAl was nearly twice as high as composite dust model estimates (Figure 5 and Table 2). Visualization of 5 day air mass back trajectories within the marine atmospheric boundary layer computed using National Oceanic and Atmospheric Administration Hybrid Single-Particle Lagrangian Integrated Trajectory model from March 2006 to April 2007 suggests that the increases in deposition seen in this region are a result of dust of Australian origin enriching air masses that then move northwestward over the south Indian subtropical gyre [*Draxler and Rolph*, 2013]. Observation of back trajectories computed several years prior to our cruise also suggests a strong seasonality in dust deposition since air masses appear to mostly interact with the Australian landmass during the Austral fall and winter while, during the rest of the year, air masses predominantly transit over oceanic regions. Both MADCOW and aerosol models thus reflect the deposition of Australian aerosols in the south Indian subtropical gyre. Composite model estimates suggest that the bulk of Australian dust is being deposited east of 90°E [*Jickells et al.*, 2005; *Mahowald et al.*, 2005] and that the northern limb of the gyre near ~12.5°S is the most impacted, consistent with our estimates (Figure 5). This is also consistent with the meridional patterns and lower surface dAl levels observed to the west of our cruise track during the GEOTRACES-JAPAN Program (see ER-11, ER-10, and ER-9; Figure 2).

Unlike composite model predictions, which are tied to a square meter of ocean surface, the MADCOW estimates are affected by the surface circulation, and this effect was particularly evident in the subtropical gyre and SECC region (see section 3.2). The lower surface dAl observed at GEOTRACES-JAPAN station ER-10 (Figure 2) suggests that the westward flowing SICC may dilute the dAl signal resulting from the deposition of Australian dust at 95°E along our cruise track. The dip in total deposition centered near 17°S may result from the advection of westward flowing SEC waters of lower dAl concentrations rather than a change in dust inputs at 17°S, since the drop coincides with a reversal of LADCP velocities (Figures 1 and 5). Farther north in the SECC domain, models predict a 15% drop in the total deposition from 12°S to 5°S, at the northernmost extent of the Australian dust plume influence. The MADCOW estimates also show a significant decline in the total deposition at that latitude, but the magnitude of the drop is significantly higher, on the order of 40% (Figure 5). The more abrupt decline in total deposition inferred from MADCOW near 12–5°S may partly be a result of the cruise track crossing the eastward flowing SECC (Figures 1 and 5), bringing dAl-depleted waters from the west. This is also consistent with the GEOTRACES-JAPAN measurements, which show surface dAl levels ~3 nM lower than our observations at station ER-9 (Figure 2), 3000.24 km to the west of our cruise track and at the northern edge of the eastward flowing SECC (Figure 1). Thus, the concentration of dAl in surface

waters of the south Indian subtropical gyre and SECC domain may be dominantly controlled by advection rather than scavenging of dAl in the mixed layer (see Figure 19 in *van Hulten et al.* [2013]). In regions where eastward flow predominates (i.e., SICC and SECC; Figure 1), our total deposition estimates may be underestimated because mixed layer dAl has been diluted with waters of lower dAl concentrations from the west (Figure 2). Accounting for this possible dilution effect in our calculations would actually exacerbate the twofold offset between our estimates of total deposition and that of composite atmospheric models in the gyre (Figure 5), suggesting that the composite model data of *Mahowald et al.* [2005] may underestimate the magnitude of total deposition along 95°E in the south Indian subtropical gyre.

Using the MADCOW dust flux for the gyre/SECC region listed in Table 2, 3.5% Fe dust content, and the geometric mean of the aerosol Fe solubility data (4.6%) of *Witt et al.* [2010] for the southwest Indian Ocean, we calculate an aeolian dFe flux of $14 \pm 8\,\mu\mathrm{mol}\,\mathrm{m}^{-2}\,\mathrm{yr}^{-1}$ (Table 3). Deposition of this flux to the $\mathrm{MLD_{OBS}}$ (47 ± 13 m) would supply 0.29 ± 0.18 nM of dFe to the mixed layer each year. However, dFe in the $\mathrm{MLD_{OBS}}$ remained remarkably uniform from the southern to northern limbs of the subtropical gyre (0.18 ± 0.03 nM, $n = 19$) in spite of the concomitant 5-fold to 11-fold increase in total dust deposition inferred from models and MADCOW, respectively (Figures 2 and 5). The lack of a noticeable enrichment in $\mathrm{MLD_{OBS}}$ dFe most likely reflects the relatively short residence time of dissolved Fe and the timing of our sampling. Air mass back trajectories suggest that the last atmospheric input of dFe likely happened 0.7 year prior to sampling when air masses that transited over Australia impacted the marine atmospheric boundary layer of the cruise track. Using our aeolian dFe flux of $14 \pm 8\,\mu\mathrm{mol}\,\mathrm{m}^{-2}\,\mathrm{yr}^{-1}$ and the inventory of dFe in the $\mathrm{MLD_{CLIM}}$ ($8.5 \pm 2.3\,\mu\mathrm{mol}\,\mathrm{m}^{-2}$), we calculate a steady state dFe residence time of 0.6 ± 0.4 year for the south Indian subtropical gyre. This short residence time suggests that any dFe signal resulting from the deposition and partial dissolution of Australian dust had probably been removed via biological uptake and inorganic scavenging by the time we sampled the region. Our dFe residence time for the south Indian subtropical gyre is comparable to the estimates of *Bergquist and Boyle* [2006] (0.1–0.4 year) and *Sarthou et al.* [2003] (<1 month) for the North Atlantic Ocean but lies at the lower end of the range of residence times estimated by *Croot et al.* [2004b] along a 10°N transection in the Atlantic (0.7–10.5 year).

4.5. Dust Deposition in the Equatorial Domain and Bay of Bengal (5°S−18°N)

The surface waters of the northeastern Indian Ocean receive dust inputs from the Indo-Gangetic alluvial plains (north and northeastern India), Southeast Asia, combined with possible long-range inputs from the Thar desert [*Kumar et al.*, 2010; *Srinivas et al.*, 2012; *Srinivas and Sarin*, 2013]. The bulk of the deposition occurs during the late northeast monsoon (January–April) and primarily consists of dry deposition because, at this time, the dominant northeasterly winds favor the transport of dry continental air over the northeastern Indian Ocean [*Srinivas and Sarin*, 2013]. Ambient aerosols within the atmospheric boundary layer of the BoB are impacted by combustion sources, with documented increases in the fractional solubility of aerosol Fe over the BoB [*Kumar et al.*, 2010].

Large discrepancies between the pattern of total deposition from MADCOW and composite dust models occurred in the equatorial regime (Figure 5). From 5°S to 5°N, models predict a factor of 3 increase in total deposition, while MADCOW estimates relatively uniform dust fluxes (Figure 5). Considering that equatorial upwelling is absent or extremely weak in the equatorial Indian Ocean [*Schott and McCreary*, 2001], we discount the possibility of equatorial upwelling reducing our calculated total dust deposition fluxes by bringing dAl-depleted waters from below into the mixed layer. It would thus appear that atmospheric models are overestimating the amount of dust originating from North Africa (see Figure 4 in *Mahowald*, 2007) or the Indian peninsular and Southeast Asia dust that is deposited into the equatorial Indian Ocean. Between 4 and 5°N, the 3.8-fold increase in total deposition inferred by MADCOW is partly an artifact of the abrupt switch from 5 to 1.1 years dAl residence time implemented in the MADCOW calculations for the BoB (see section 4.1). Nevertheless, starting at 5°N, surface dAl also shows a significant increase from 7.15 nM at 5°N to ~12 nM at 10°N (Figure 2), consistent with increasing dust fluxes northward. We note, however, that surface dAl as far as 6°N might have been impacted by the eastward flowing SMC, which could carry dAl-enriched waters (~10 nM) from the Arabian Sea region across the cruise track [*Measures and Vink*, 1999; *Vinayachandran et al.*, 1999]. Nevertheless, in the southern BoB (5–10°N), the total deposition estimates of MADCOW were not significantly different from that of dust models (Mann-Whitney U test) and lie in the middle of the range of recent shipboard aerosol sampling campaign estimations (Table 2).
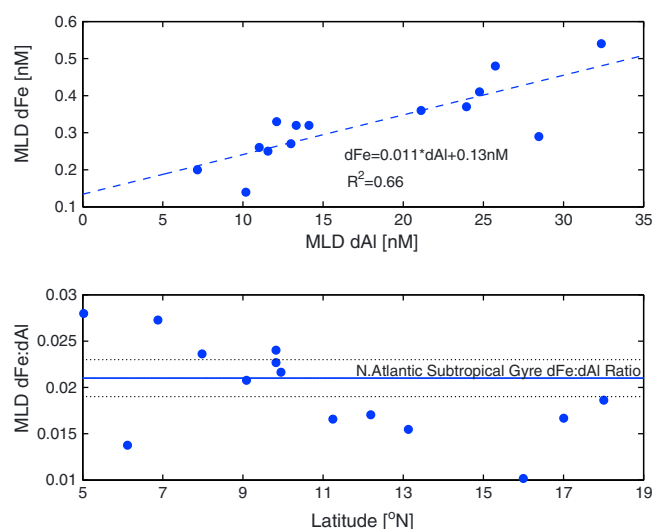
Figure 6. Relationship between (top) MLD_{OBS} dAl and dFe in the Bay of Bengal and (bottom) dFe:dAl ratio in the BoB MLD_{OBS}. The dashed line in Figure 6 (top) shows the linear regression between dFe and dAl ($dFe = 0.011 \pm 0.002 \times dAl + 0.13 \pm 0.03$). The full and dashed lines in Figure 6 (bottom) represent the mean $\pm 1\sigma$ dFe:dAl ratio observed in the North Atlantic subtropical gyre [*Hatta et al.*, 2014]. Note that the two stations influenced by eddy pumping were removed to produce these plots (see text for details).

Assuming that the ambient aerosols in the southern BoB contain 3.5% Fe by weight and using the mean MADCOW total dust deposition flux for the southern BoB listed in Table 2, we estimate a total aeolian Fe flux to the BoB of $90 \pm 20\,\mathrm{mg\,m^{-2}\,yr^{-1}}$, which is lower than the dry deposition Fe flux of *Srinivas and Sarin* [2013] of $140\,\mathrm{mg\,m^{-2}\,yr^{-1}}$ based on the analysis of ambient BoB aerosols sampled during the period of continental outflow. The higher Fe deposition flux of *Srinivas and Sarin* [2013] could result from the fact that the marine atmospheric boundary layer of the BoB is impacted by combustion products [*Kumar et al.*, 2010], which may have a higher Fe content than the average continental crust material that we used in our estimates. Using the geometric mean of *Kumar et al.*'s [2010] fractional solubility measurements of aerosol Fe in the marine boundary layer of the BoB (18%), we calculate an aeolian dFe flux of

$290 \pm 70\,\mathrm{\mu mol\,m^{-2}\,yr^{-1}}$ to surface waters of the BoB (Table 3), comparable to the mean aeolian dFe flux of $\sim 300\,\mathrm{\mu mol\,m^{-2}\,yr^{-1}}$ estimated in the eastern Atlantic under the influence of the Saharan dust plume [*Sarthou et al.*, 2003]. Based on the inventory of dFe measured in the MLD_{CLIM} ($25 \pm 4\,\mathrm{m}$) of the BoB ($9.2 \pm 3.5\,\mathrm{\mu mol\,m^{-2}}$), we estimate that the steady state residence time of dFe in surface waters of the BoB with respect to atmospheric deposition is 12 ± 5 days. The mixed layer dFe levels of the BoB are thus expected to show considerable short-term variations due to rapid removal through active biological uptake, passive scavenging, and/or colloidal aggregation as well as the pronounced seasonality of the dust inputs impacting the BoB.

Unlike any other locations along the cruise track, dFe and dAl were positively correlated in the mixed layer of the BoB (Figure 6), illustrating that these elements share common atmospheric and riverine source terms. Figure 6 (bottom) displays the dFe:dAl ratios as a function of latitude in the mixed layer of the BoB overlaid with the mean $\pm 1\sigma$ ratio that *Hatta et al.* [2014] recently observed in the Saharan dust impacted North Atlantic subtropical gyre. Interestingly, the dFe:dAl ratios in the mixed layer of the BoB show a north-south divide, with ratios generally less than that observed underneath the Saharan dust plume in the northern BoB (>10°N) and higher to the south (Figure 6). Although north-south gradients in the composition of dust or solubility of aerosol trace elements in the BoB could produce a meridional gradient in the ratios of dFe:dAl, the lower dFe:dAl ratios observed in the northern BoB (>10°N) are also consistent with a greater influence of the Ganges-Brahmaputra river plume on the distribution of surface dFe and dAl in the northern BoB (see section 4.2). Perhaps the greater reactivity of fluvial Fe toward the particulate phase relative to Al during estuarine mixing produces lower dFe:dAl ratios in surface waters of the northern BoB. In the southern BoB (<10°N), the fact that most dFe:dAl ratios cluster on or above that observed in the subtropical North Atlantic could reflect the dominance of aerosol deposition in controlling surface dFe and dAl. In other words, we surmise that the changing dFe:dAl ratios may be diagnostic of the primary supply of trace elements to surface waters of the BoB: aerosols in the southern BoB (<10°N) yielding elevated dFe:dAl and riverine inputs in the northern BoB (>10°N) producing lower dFe:dAl ratios.

5. Conclusions

High-resolution sampling for trace elements during the U.S. CLIVAR I08S and I09N sections has produced an unprecedented picture of the distribution of dissolved Al and Fe in surface waters of the eastern Indian

Ocean. Dissolved Fe (dFe) and Al (dAl) show remarkable meridional concentration gradients, which reflect the differing input sources and residence times characterizing each element across the contrasting hydrographic regimes encountered along this section. In the eastern Indian sector of the Southern Ocean, the distributions of dAl and dFe confirm that aeolian inputs of dFe are negligible and that upwelling/deep mixing are the predominant input routes of dFe to the mixed layer. In the south Indian subtropical gyre along 95°E, the transport and deposition of Australian dust produce a northward increase in surface dAl from ~30°S to 18°S. However, dFe levels remained relatively constant, presumably because the residence time of dFe in the gyre was equal to or shorter than the 0.7 year lag between sampling and the latest possible dust inputs inferred from air mass back trajectories. In the northern Bay of Bengal (>10°N), freshwater inputs from the Ganges-Brahmaputra river system impact the distribution of dAl. This riverine source combines with dust deposition emanating from the Indo-Gangetic plains and Southeast Asia to produce the highest surface dAl levels observed on the section and a northward increase in dFe from 5°N to 18°N.

This work also provides new constraints on atmospheric model outputs of total dust deposition in the eastern Indian Ocean. In this regard, we have produced 75 independent total dust deposition estimates and find that the composite model of *Mahowald et al.* [2005] produces meridional patterns of dust deposition in the eastern Indian Ocean that are comparable to that inferred from the distribution of dAl in the climatological mixed layer within a factor of 0.4 to 4.2. The largest discrepancies in the magnitude of the fluxes occurred in the south Indian subtropical gyre and equatorial domain, while the Southern Ocean and southern Bay of Bengal estimates were in good agreement.

More measurements of the fractional solubility of aerosol Al are required, particularly in regions of low deposition such as the Southern Ocean, to reduce the uncertainty inherent to calculations that use the concentration of lithogenic elements in the mixed layer as a proxy of dust deposition. In addition, while this work shows that some atmospheric models produce a reasonable approximation of total dust deposition in the eastern Indian Ocean, translating this information into a flux of dissolved Fe still requires a better understanding of the factors controlling the solubility of aerosol Fe during atmospheric transport and deposition. Our estimates would also be greatly improved if one could determine regional variations of the residence time of dAl in the surface ocean independent of atmospheric model estimates of total dust deposition and short-term aerosol sampling campaigns, perhaps as a function of the suspended particulate load and/or export production in the mixed layer.

References

Baker, A. R., and P. L. Croot (2010), Atmospheric and marine controls on aerosol iron solubility in seawater, *Mar. Chem.*, *120*, 4–13, doi:10.1016/j.marchem.2008.09.003.

Baker, A. R., T. D. Jickells, M. Witt, and K. L. Linge (2006), Trends in the solubility of iron, aluminum, manganese and phosphorus in aerosol collected over the Atlantic Ocean, *Mar. Chem.*, *98*, 43–58, doi:10.1016/j.marchem.2005.06.004.

Benshila, R., F. Durand, S. Masson, R. Bourdallé-Badie, C. de Boyer Montégut, F. Papa, and G. Madec (2014), The upper Bay of Bengal salinity structure in a high-resolution model, *Ocean Model.*, *74*, 36–52, doi:10.1016/j.ocemod.2013.12.001.

Bergquist, B. A., and E. A. Boyle (2006), Dissolved iron in the tropical and subtropical Atlantic Ocean, *Global Biogeochem. Cycles*, *20*, GB1015, doi:10.1029/2005GB002505.

Blain, S., et al. (2001), A biogeochemical study of the island mass effect in the context of the iron hypothesis: Kerguelen Islands, Southern Ocean, *Deep Sea Res., Part I*, *48*, 163–187, doi:10.1016/S0967-0637(00)00047-9.

Blain, S., G. Sarthou, and P. Laan (2008), Distribution of dissolved iron during the natural iron-fertilization experiment KEOPS (Kerguelen Plateau, Southern Ocean), *Deep Sea Res., Part II*, *55*(5–7), 594–605, doi:10.1016/j.dsr2.2007.12.028.

Bowie, A. R., D. Lannuzel, T. A. Remenyi, T. Wagener, P. J. Lam, P. W. Boyd, C. Guieu, A. T. Townsend, and T. W. Trull (2009), Biogeochemical iron budgets of the Southern Ocean south of Australia: Decoupling of iron and nutrient cycles in the subantarctic zone by the summertime supply, *Global Biogeochem. Cycles*, *23*, GB4034, doi:10.1029/2009GB003500.

Boyd, P. W., and D. Mackie (2008), Comment on "The Southern Ocean biological response to aeolian iron deposition", *Science*, *319*, 159, doi:10.1126/science.1149884.

Boyd, P., et al. (2007), Mesoscale Iron Enrichment Experiments 1993–2005: Synthesis and future directions, *Science*, *315*, 612–617, doi:10.1126/science.1131669.

Bucciarelli, E., S. Blain, and P. Tréguer (2001), Iron and manganese in the wake of the Kerguelen Islands (Southern Ocean), *Mar. Chem.*, *73*(1), 21–36, doi:10.1016/S0304-4203(00)00070-0.

Buck, C. S., W. M. Landing, J. A. Resing, and C. I. Measures (2010), The solubility and deposition of aerosol Fe and other trace elements in the North Atlantic Ocean: Observations from the A16N CLIVAR/CO2 repeat hydrography section, *Mar. Chem.*, *120*, 57–70, doi:10.1016/j.marchem.2008.08.003.

Buck, C. S., W. M. Landing, and J. A. Resing (2013), Pacific Ocean aerosols: Deposition and solubility of iron, aluminum, and other trace elements, *Mar. Chem.*, *157*, 117–130, doi:10.1016/j.marchem.2013.09.005.

Cassar, N., M. L. Bender, B. A. Barnett, S. Fan, W. Moxim, H. Levy II, and B. Tilbrook (2007), The Southern Ocean response to aeolian iron deposition, *Science*, *317*(5841), 1067–1070, doi:10.1126/science.1144602.

Chever, F., G. Sarthou, E. Bucciarelli, S. Blain, and A. R. Bowie (2010), An iron budget during the natural iron fertilization experiment KEOPS (Kerguelen Islands, Southern Ocean), *Biogeosciences*, *7*, 455–468, doi:10.5194/bg-7-455-2010.

Croot, P. L., K. Andersson, M. Öztürk, and D. R. Turner (2004a), The distribution and speciation of iron along 6°E in the Southern Ocean, *Deep Sea Res., Part II, 51*, 2857–2879, doi:10.1016/j.dsr2.2003.10.012.

Croot, P. L., P. Streu, and A. R. Baker (2004b), Short residence time for iron in surface seawater impacted by atmospheric dry deposition from Saharan dust events, *Geophys. Res. Lett., 31*, L23S08, doi:10.1029/2004GL020153.

Dammshäuser, A., T. Wagener, and P. L. Croot (2011), Surface water dissolved aluminum and titanium: Tracers for specific time scales of dust deposition to the Atlantic?, *Geophys. Res. Lett., 38*, L24601, doi:10.1029/2011GL049847.

de Baar, H. J. W., J. T. M. de Jong, D. C. E. Bakker, B. M. Löscher, C. Veth, U. Bathmann, and V. Smetacek (1995), Importance of iron for plankton blooms and carbon dioxide drawdown in the Southern Ocean, *Nature, 373*(6513), 412–415, doi:10.1038/373412a0.

de Boyer Montégut, C. (2004), Mixed layer depth over the global ocean: An examination of profile data and a profile-based climatology, *J. Geophys. Res., 109*, C12003, doi:10.1029/2004JC002378.

de Jong, J., V. Schoemann, D. Lannuzel, P. Croot, H. de Baar, and J.-L. Tison (2012), Natural iron fertilization of the Atlantic sector of the Southern Ocean by continental shelf sources of the Antarctic Peninsula, *J. Geophys. Res., 117*, G01029, doi:10.1029/2011JG001679.

Draxler, R., and G. Rolph (2013), HYSPLIT (HYbrid Single-Particle Lagrangian Integrated Trajectory) Model access via NOAA ARL READY website, *NOAA Air Resour. Lab. Coll. Park. MD*. [Available at http://www.arl.noaa.gov/HYSPLIT.php (Accessed 1 November 2013).]

Duce, R., et al. (1991), The atmospheric input of trace species to the world ocean, *Global Biogeochem. Cycles, 5*(3), 193–259, doi:10.1029/91GB01778.

Falkowski, P. G., R. T. Barber, and V. Smetacek (1998), Biogeochemical controls and feedbacks on ocean primary production, *Science, 281*, 200–206, doi:10.1126/science.281.5374.200.

Fan, S., W. J. Moxim, and H. L. Levy (2006), Aeolian input of bioavailable iron to the ocean, *Geophys. Res. Lett., 33*, L07602, 2–5, doi:10.1029/2005GL024852.

Gao, Y., G. Xu, J. Zhan, J. Zhang, W. Li, Q. Lin, L. Chen, and H. Lin (2013), Spatial and particle size distributions of atmospheric dissolvable iron in aerosols and its input to the Southern Ocean and coastal East Antarctica, *J. Geophys. Res. Atmos., 118*, 12,634–12,648, doi:10.1002/2013JD020367.

Gaudichet, A., R. Lefevre, A. Gaudry, B. Ardouin, G. Lambert, and J. M. Miller (1989), Mineralogical composition of aerosols at Amsterdam Island, *Tellus B, 41B*(3), 344–352, doi:10.1111/j.1600-0889.1989.tb00313.x.

Gordon, A. L., S. Ma, D. B. Olson, P. Hacker, A. Ffield, L. D. Talley, D. Wilson, and M. Baringer (1997), Advection and diffusion of Indonesian Throughflow Water within the Indian Ocean South Equatorial Current, *Geophys. Res. Lett., 24*(21), 2573–2576, doi:10.1029/97GL01061.

Grand, M. M., C. Buck, W. Landing, C. I. Measures, M. Hatta, W. Hiscock, M. Brown, and J. Resing (2014), Quantifying the impact of atmospheric deposition on the biogeochemistry of Fe and Al in the upper ocean: A decade of collaboration with the U.S. CLIVAR-CO$_2$ Repeat Hydrography Program, *Oceanography, 27*(1), 62–65, doi:10.5670/oceanog.2014.08.

Grand, M. M., C. I. Measures, M. Hatta, W. T. Hiscock, W. M. Landing, P. L. Morton, C. S. Buck, P. M. Barrett, and J. A. Resing (2015), Dissolved Fe and Al in the upper 1000m of the eastern Indian Ocean: a high-resolution transect from the Antarctic margin to the Bay of Bengal, *Global Biogeochem. Cycles*, doi:10.1002/2014GB004920.

Han, Q., J. K. Moore, C. Zender, C. Measures, and D. Hydes (2008), Constraining oceanic dust deposition using surface ocean dissolved Al, *Global Biogeochem. Cycles, 22*, GB2003, doi:10.1029/2007GB002975.

Han, Q., C. S. Zender, J. K. Moore, C. S. Buck, Y. Chen, A. Johansen, and C. I. Measures (2012), Global estimates of mineral dust aerosol iron and aluminum solubility that account for particle size using diffusion-controlled and surface-area-controlled approximations, *Global Biogeochem. Cycles, 26*, GB2038, doi:10.1029/2011GB004186.

Hatta, M., C. I. Measures, K. Selph, M. Zhou, J. Yang, and W. Hiscock (2013), Iron fluxes from the shelf regions near the South Shetland Islands in the Drake Passage during the austral-winter 2006, *Deep Sea Res., Part II, 90*, 89–101, doi:10.1016/j.dsr2.2012.11.003.

Hatta, M., C. I. Measures, J. Wu, S. Roshan, J. N. Fitzsimmons, P. Sedwick, and P. Morton (2014), An overview of dissolved Fe and Mn Distributions during the 2010–2011 U.S. GEOTRACES North Atlantic Cruises: GEOTRACES GA03, *Deep Sea Res., Part II*, doi:10.1016/j.dsr2.2014.07.005.

Hayes, C. T., R. F. Anderson, M. Q. Fleisher, S. Serno, G. Winckler, and R. Gersonde (2013), Quantifying lithogenic inputs to the North Pacific Ocean using the long-lived thorium isotopes, *Earth Planet. Sci. Lett., 383*, 16–25, doi:10.1016/j.epsl.2013.09.025.

Heimburger, A., R. Losno, S. Triquet, F. Dulac, and N. Mahowald (2012), Direct measurements of atmospheric iron, cobalt, and aluminum-derived dust deposition at Kerguelen Islands, *Global Biogeochem. Cycles, 26*, GB4016, doi:10.1029/2012GB004301.

Heimburger, A., R. Losno, and S. Triquet (2013a), Solubility of iron and other trace elements in rainwater collected on the Kerguelen Islands (South Indian Ocean), *Biogeosciences, 10*(10), 6617–6628, doi:10.5194/bg-10-6617-2013.

Heimburger, A., R. Losno, S. Triquet, and E. B. Nguyen (2013b), Atmospheric deposition fluxes of 26 elements over the Southern Indian Ocean: Time series on Kerguelen and Crozet Islands, *Global Biogeochem. Cycles, 27*, 440–449, doi:10.1002/gbc.20043.

Holte, J., J. Gilson, L. Talley, and D. Roemmich (2010), Argo Mixed Layers, Scripps Institution of Oceanography/UCSD. [Available at http://mixedlayer.ucsd.edu (Accessed 15 October 2013).]

Hoppema, M., H. J. W. de Baar, E. Fahrbach, H. H. Hellmer, and B. Klein (2003), Substantial advective iron loss diminishes phytoplankton production in the Antarctic Zone, *Global Biogeochem. Cycles, 17*(1), 1025, doi:10.1029/2002GB001957.

Hsieh, Y.-T., G. M. Henderson, and A. L. Thomas (2011), Combining seawater 232Th and 230Th concentrations to determine dust fluxes to the surface ocean, *Earth Planet. Sci. Lett., 312*(3–4), 280–290, doi:10.1016/j.epsl.2011.10.022.

Jickells, T. (1999), The inputs of dust derived elements to the Sargasso Sea: A synthesis, *Mar. Chem., 68*, 5–14, doi:10.1016/S0304-4203(99)00061-4.

Jickells, T. D., et al. (2005), Global iron connections between desert dust, ocean biogeochemistry, and climate, *Science, 308*(5718), 67–71, doi:10.1126/science.1105959.

Klunder, M. B., P. Laan, R. Middag, H. J. W. De Baar, and J. V. Ooijen (2011), Dissolved iron in the Southern Ocean (Atlantic sector), *Deep Sea Res., Part II, 58*, 2678–2694, doi:10.1016/j.dsr2.2010.10.042.

Kumar, A., M. M. Sarin, and B. Srinivas (2010), Aerosol iron solubility over Bay of Bengal: Role of anthropogenic sources and chemical processing, *Mar. Chem., 121*(1–4), 167–175, doi:10.1016/j.marchem.2010.04.005.

Lancelot, C., A. de Montety, H. Goosse, S. Becquevort, V. Schoemann, B. Pasquer, and M. Vancoppenolle (2009), Spatial distribution of the iron supply to phytoplankton in the Southern Ocean: A model study, *Biogeosciences, 6*(12), 2861–2878, doi:10.5194/bg-6-2861-2009.

Lannuzel, D., V. Schoemann, J. de Jong, J.-L. Tison, and L. Chou (2007), Distribution and biogeochemical behavior of iron in the East Antarctic sea ice, *Mar. Chem., 106*, 18–32, doi:10.1016/j.marchem.2006.06.010.

Lannuzel, D., V. Schoemann, J. de Jong, B. Pasquer, P. van der Merwe, F. Masson, J.-L. Tison, and A. Bowie (2010), Distribution of dissolved iron in Antarctic sea ice: Spatial, seasonal, and interannual variability, *J. Geophys. Res., 115*, G03022, doi:10.1029/2009JG001031.

Lannuzel, D., A. R. Bowie, T. Remenyi, P. Lam, A. Townsend, E. Ibisanmi, E. Butler, T. Wagener, and V. Schoemann (2011), Distributions of dissolved and particulate iron in the sub-Antarctic and Polar Frontal Southern Ocean (Australian sector), *Deep Sea Res., Part II, 58*, 2094–2112, doi:10.1016/j.dsr2.2011.05.027.

Lin, H., S. Rauschenberg, C. R. Hexel, T. J. Shaw, and B. S. Twining (2011), Free-drifting icebergs as sources of iron to the Weddell Sea, *Deep Sea Res., Part II, 58*, 1392–1406, doi:10.1016/j.dsr2.2010.11.020.

Mahowald, N. M. (2007), Anthropocene changes in desert area: Sensitivity to climate model predictions, *Geophys. Res. Lett., 34*, L18817, doi:10.1029/2007GL030472.

Mahowald, N. M., A. R. Baker, G. Bergametti, N. Brooks, R. A. Duce, T. D. Jickells, N. Kubilay, J. M. Prospero, and I. Tegen (2005), Atmospheric global dust cycle and iron inputs to the ocean, *Global Biogeochem. Cycles, 19*, GB4025, doi:10.1029/2004GB002402.

Measures, C. I., and E. Brown (1996), Estimating dust input to the Atlantic ocean using surface water aluminum concentrations, in *The Impact of Desert Dust Across the Mediterranean*, edited by S. Guerzoni and R. Chester, pp. 301–311, Kluwer Acad., Dordrecht, Netherlands.

Measures, C. I., and S. Vink (1999), Seasonal variations in the distribution of Fe and Al in the surface waters of the Arabian Sea, *Deep Sea Res., Part II, 46*, 1597–1622.

Measures, C. I., and S. Vink (2000), On the use of dissolved aluminum in surface waters to estimate dust deposition to the ocean, *Global Biogeochem. Cycles, 14*(1), 317–327, doi:10.1029/1999GB001188.

Measures, C. I., and S. Vink (2001), Dissolved Fe in the upper waters of the Pacific sector of the Southern Ocean, *Deep Sea Res., Part II, 48*, 3913–3941, doi:10.1016/S0967-0645(01)00074-1.

Measures, C. I., J. Yuan, and J. A. Resing (1995), Determination of iron in seawater by flow injection analysis using in-line preconcentration and spectrophotometric detection, *Mar. Chem., 50*, 1–10.

Measures, C. I., W. M. Landing, M. T. Brown, and C. S. Buck (2008a), A commercially available rosette system for trace metal clean sampling, *Limnol. Oceanogr. Methods, 6*, 384–394.

Measures, C. I., W. M. Landing, M. T. Brown, and C. S. Buck (2008b), High-resolution Al and Fe data from the Atlantic Ocean CLIVAR-CO 2 Repeat Hydrography A16N transect: Extensive linkages between atmospheric dust and upper ocean geochemistry, *Global Biogeochem. Cycles, 22*, GB1005, doi:10.1029/2007GB003042.

Measures, C. I., T. Sato, S. Vink, S. Howell, and Y. H. Li (2010), The fractional solubility of aluminum from mineral aerosols collected in Hawaii and implications for atmospheric deposition of biogeochemically important trace elements, *Mar. Chem., 120*, 144–153, doi:10.1016/j.marchem.2009.01.014.

Measures, C. I., M. T. Brown, K. E. Selph, A. Apprill, M. Zhou, M. Hatta, and W. T. Hiscock (2013), The influence of shelf processes in delivering dissolved iron to the HNLC waters of the Drake Passage, Antarctica, *Deep Sea Res., Part II, 90*, 77–88, doi:10.1016/j.dsr2.2012.11.004.

Measures, C., M. Hatta, and M. M. (2012), Bioactive Trace Metal Distributions and Biogeochemical Controls in the Southern Ocean, *Oceanography, 25*(3), 122–133, doi:10.5670/oceanog.2012.85.

Meybeck, M. (1988), How to establish and use world budgets of riverine materials, in *Physical and Chemical Weathering in Geochemical Cycles*, edited by A. Lerman and M. Meybeck, pp. 247–272, Kluwer Acad., Dordrecht, Netherlands.

Middag, R., C. van Slooten, H. J. W. de Baar, and P. Laan (2011), Dissolved aluminum in the Southern Ocean, *Deep Sea Res., Part II, 58*, 2647–2660, doi:10.1016/j.dsr2.2011.03.001.

Middag, R., H. J. W. de Baar, P. Laan, and O. Huhn (2012), The effects of continental margins and water mass circulation on the distribution of dissolved aluminum and manganese in Drake Passage, *J. Geophys. Res., 117*, C01019, doi:10.1029/2011JC007434.

Middag, R., H. J. W. de Baar, M. B. Klunder, and P. Laan (2013), Fluxes of dissolved aluminum and manganese to the Weddell Sea and indications for manganese co-limitation, *Limnol. Oceanogr., 58*(1), 287–300, doi:10.4319/lo.2013.58.1.0287.

Moore, C., et al. (2009), Large-scale distribution of Atlantic nitrogen fixation controlled by iron availability, *Nat. Geosci., 2*(12), 867–871, doi:10.1038/ngeo667.

Moore, J. K., and O. Braucher (2008), Sedimentary and mineral dust sources of dissolved iron to the world ocean, *Biogeosciences, 5*, 631–656, doi:10.5194/bg-5-631-2008.

Moran, S., and R. Moore (1992), Kinetics of the removal of dissolved aluminum by diatoms in seawater: A comparison with thorium, *Geochim. Cosmochim. Acta, 56*, 3365–3374, doi:10.1016/0016-7037(92)90384-U.

Muraleedharan, K. R., P. Jasmine, C. T. Achuthankutty, C. Revichandran, P. K. Dinesh Kumar, P. Anand, and G. Rejomon (2007), Influence of basin-scale and mesoscale physical processes on biological productivity in the Bay of Bengal during the summer monsoon, *Prog. Oceanogr., 72*(4), 364–383, doi:10.1016/j.pocean.2006.09.012.

Nishioka, J., H. Obata, and D. Tsumune (2013), Evidence of an extensive spread of hydrothermal dissolved iron in the Indian Ocean, *Earth Planet. Sci. Lett., 361*, 26–33, doi:10.1016/j.epsl.2012.11.040.

Obata, H., Y. Nozaki, D. S. Alibo, and Y. Yamamoto (2004), Dissolved Al, In, and Ce in the eastern Indian Ocean and the Southeast Asian Seas in comparison with the radionuclides 210 Pb and 210 Po, *Geochim. Cosmochim. Acta, 68*(5), 1035–1048, doi:10.1016/j.gca.2003.07.021.

Orsi, A. H., T. I. I. I. Whitworth, and W. D. J. Nowlin (1995), On the meridional extent and fronts of the Antarctic Circumpolar Current, *Deep Sea Res., Part I, 42*, 641–673, doi:10.1016/0967-0637(95)00021-W.

Palastanga, V., P. J. van Leeuwen, M. W. Schouten, and W. P. M. de Ruijter (2007), Flow structure and variability in the subtropical Indian Ocean: Instability of the South Indian Ocean Countercurrent, *J. Geophys. Res., 112*, C01001, doi:10.1029/2005JC003395.

Planquette, H., et al. (2007), Dissolved iron in the vicinity of the Crozet Islands, Southern Ocean, *Deep Sea Res., Part II, 54*(18–20), 1999–2019, doi:10.1016/j.dsr2.2007.06.019.

Planquette, H., R. R. Sanders, P. J. Statham, P. J. Morris, and G. R. Fones (2011), Fluxes of particulate iron from the upper ocean around the Crozet Islands: A naturally iron-fertilized environment in the Southern Ocean, *Global Biogeochem. Cycles, 25*, GB2011, doi:10.1029/2010GB003789.

Prasanna Kumar, S., P. Muraleedharan, T. Prasad, M. Gauns, N. Ramaiah, S. de Souza, S. Sardesai, and M. Madhupratap (2002), Why is the Bay of Bengal less productive during summer monsoon compared to the Arabian Sea?, *Geophys. Res. Lett., 29*(24), 2235, doi:10.1029/2002GL016013.

Prasanna Kumar, S., M. Nuncio, and J. Narvekar (2004), Are eddies nature's trigger to enhance biological productivity in the Bay of Bengal?, *Geophys. Res. Lett., 31*, L07309, doi:10.1029/2003GL019274.

Prasanna Kumar, S., M. Nuncio, N. Ramaiah, S. Sardesai, J. Narvekar, V. Fernandes, and J. T. Paul (2007), Eddy-mediated biological productivity in the Bay of Bengal during fall and spring intermonsoons, *Deep Sea Res., Part I, 54*(9), 1619–1640, doi:10.1016/j.dsr.2007.06.002.

Ramaswamy, V., B. Vijay Kumar, G. Parthiban, V. Ittekkot, and R. R. Nair (1997), Lithogenic fluxes in the Bay of Bengal measured by sediment traps, *Deep Sea Res., Part I, 44*(5), 793–810, doi:10.1016/S0967-0637(96)00117-3.

Reid, J. L. (2003), On the total geostrophic circulation of the Indian Ocean: Flow patterns, tracers, and transports, *Prog. Oceanogr., 56*, 137–186, doi:10.1016/S0079-6611(02)00141-6.

Resing, J. A., and C. I. Measures (1994), Fluorometric determination of Al in seawater by flow injection analysis with in-line preconcentration, *Anal. Chem., 66*, 4105–4111, doi:10.1021/ac00094a039.

Rintoul, S. R., and J. L. Bullister (1999), A late winter hydrographic section from Tasmania to Antarctica, *Deep Sea Res., Part I, 46*(8), 1417–1454, doi:10.1016/S0967-0637(99)00013-8.

Sardessai, S., N. Ramaiah, S. P. Kumar, and S. N. De Sousa (2007), Influence of environmental forcings on the seasonality of dissolved oxygen and nutrients in the Bay of Bengal, *J. Mar. Res.*, 65, 301–316.

Sarthou, G., et al. (2003), Atmospheric iron deposition and sea-surface dissolved iron concentrations in the eastern Atlantic Ocean, *Deep Sea Res., Part I*, 50(10–11), 1339–1352, doi:10.1016/S0967-0637(03)00126-2.

Sato, T. (2002), Determining the fractional solubility in seawater of aluminum derived from atmospheric aerosols, MS thesis, Univ. of Hawaii.

Schott, F. A., and J. P. McCreary (2001), The monsoon circulation of the Indian Ocean, *Prog. Oceanogr.*, 51(1), 1–123, doi:10.1016/S0079-6611 (01)00083-0.

Schüßler, U., W. Balzer, and A. Deeken (2005), Dissolved Al distribution, particulate Al fluxes and coupling to atmospheric Al and dust deposition in the Arabian Sea, *Deep Sea Res., Part II*, 52(14–15), 1862–1878, doi:10.1016/j.dsr2.2005.06.005.

Sholkovitz, E. R., P. N. Sedwick, T. M. Church, A. R. Baker, and C. F. Powell (2012), Fractional solubility of aerosol iron: Synthesis of a global-scale data set, *Geochim. Cosmochim. Acta*, 89, 173–189, doi:10.1016/j.gca.2012.04.022.

Siedler, G., M. Rouault, and J. R. E. Lutjeharms (2006), Structure and origin of the subtropical South Indian Ocean Countercurrent, *Geophys. Res. Lett.*, 33, L24609, doi:10.1029/2006GL027399.

Sokolov, S., and S. R. Rintoul (2007), On the relationship between fronts of the Antarctic Circumpolar Current and surface chlorophyll concentrations in the Southern Ocean, *J. Geophys. Res.*, 112, C07030, doi:10.1029/2006JC004072.

Srinivas, B., and M. M. Sarin (2013), Atmospheric dry-deposition of mineral dust and anthropogenic trace metals to the Bay of Bengal, *J. Mar. Syst.*, 126, 56–68, doi:10.1016/j.jmarsys.2012.11.004.

Srinivas, B., M. M. Sarin, and A. Kumar (2012), Impact of anthropogenic sources on aerosol iron solubility over the Bay of Bengal and the Arabian Sea, *Biogeochemistry*, 110(1–3), 257–268, doi:10.1007/s10533-011-9680-1.

Stoll, H. M., A. Arevalos, A. Burke, P. Ziveri, G. Mortyn, N. Shimizu, and D. Unger (2007), Seasonal cycles in biogenic production and export in Northern Bay of Bengal sediment traps, *Deep Sea Res., Part II*, 54, 558–580, doi:10.1016/j.dsr2.2007.01.002.

Tagliabue, A., L. Bopp, and O. Aumont (2009), Evaluating the importance of atmospheric and sedimentary iron sources to Southern Ocean biogeochemistry, *Geophys. Res. Lett.*, 36, L13601, doi:10.1029/2009GL038914.

Tagliabue, A., T. Mtshali, O. Aumont, A. R. Bowie, M. B. Klunder, A. N. Roychoudhury, and S. Swart (2012), A global compilation of dissolved iron measurements: Focus on distributions and processes in the Southern Ocean, *Biogeosciences*, 9(6), 2333–2349, doi:10.5194/bg-9-2333-2012.

Tagliabue, A., O. Aumont, and L. Bopp (2014a), The impact of different external sources of iron on the global carbon cycle, *Geophys. Res. Lett.*, 41, 920–926, doi:10.1002/2013GL059059.

Tagliabue, A., J.-B. Sallée, A. R. Bowie, M. Lévy, S. Swart, and P. W. Boyd (2014b), Surface-water iron supplies in the Southern Ocean sustained by deep winter mixing, *Nat. Geosci.*, 7(4), 314–320, doi:10.1038/ngeo2101.

Talley, L. D., G. L. Pickard, W. J. Emery, and J. H. Swift (2011), *Descriptive Physical Oceanography: An Introduction*, 6th ed., Elsevier Inc., Oxford, U. K.

Tanaka, T. Y., and M. Chiba (2006), A numerical study of the contributions of dust source regions to the global dust budget, *Global Planet. Change*, 52(1–4), 88–104, doi:10.1016/j.gloplacha.2006.02.002.

Tréguer, P., D. M. Nelson, A. J. Van Bennekom, D. J. Demaster, A. Leynaert, and B. Quéguiner (1995), The silica balance in the world ocean: A reestimate, *Science*, 268(5209), 375–9, doi:10.1126/science.268.5209.375.

van Beusekom, J. E. E., A. J. V. Van Bennekom, J. Morvans, P. Treguer, and J. Morvan (1997), Aluminum and silicic acid in water and sediments of the Enderby and Crozet Basins, *Deep Sea Res., Part II*, 44(5), 987–1003, doi:10.1016/S0967-0645(96)00105-1.

van Hulten, M. M. P., A. Sterl, A. Tagliabue, J.-C. Dutay, M. Gehlen, H. J. W. de Baar, and R. Middag (2013), Aluminium in an ocean general circulation model compared with the West Atlantic Geotraces cruises, *J. Mar. Syst.*, 126, 3–23, doi:10.1016/j.jmarsys.2012.05.005.

Vinayachandran, P. N., and J. Kurian (2007), Hydrographic observations and model simulation of the Bay of Bengal freshwater plume, *Deep Sea Res., Part I*, 54(4), 471–486, doi:10.1016/j.dsr.2007.01.007.

Vinayachandran, P., Y. Masumoto, T. Mikawa, and T. Yamagata (1999), Intrusion of the Southwest Monsoon Current into the Bay of Bengal, *J. Geophys. Res.*, 104(C5), 11,077–11,085, doi:10.1029/1999JC900035.

Vu, H. T. D., and Y. Sohrin (2013), Diverse stoichiometry of dissolved trace metals in the Indian Ocean, *Sci. Rep.*, 3, 1745, doi:10.1038/srep01745.

Wadley, M. R., T. D. Jickells, and K. J. Heywood (2014), The role of iron sources and transport for Southern Ocean productivity, *Deep Sea Res., Part I*, 87, 82–94, doi:10.1016/j.dsr.2014.02.003.

Wagener, T., C. Guieu, R. Losno, S. Bonnet, and N. Mahowald (2008), Revisiting atmospheric dust export to the Southern Hemisphere ocean: Biogeochemical implications, *Global Biogeochem. Cycles*, 22, GB2006, doi:10.1029/2007GB002984.

Witt, M. L. I., T. A. Mather, A. R. Baker, J. C. M. De Hoog, and D. M. Pyle (2010), Atmospheric trace metals over the south-west Indian Ocean: Total gaseous mercury, aerosol trace metal concentrations and lead isotope ratios, *Mar. Chem.*, 121(1–4), 2–16, doi:10.1016/j.marchem.2010.02.005.

Wong, A. P. S. (2005), Subantarctic Mode Water and Antarctic Intermediate Water in the South Indian Ocean based on profiling float data 2000–2004, *J. Mar. Res.*, 63(4), 789–812, doi:10.1357/0022240054663196.

Wuttig, K., T. Wagener, M. Bressac, A. Dammshäuser, P. Streu, C. Guieu, and P. L. Croot (2013), Impacts of dust deposition on dissolved trace metal concentrations (Mn, Al and Fe) during a mesocosm experiment, *Biogeosciences*, 10(4), 2583–2600, doi:10.5194/bg-10-2583-2013.